ISSN (Print) 1226-1750
ISSN (Online) 2233-6656
Journal of Magnetics 30(4), 889-896 (2025) https://doi.org/10.4283/JMAG.2025.30.4.889

Optimization of $LaBr_3$(Ce) Scintillator Parameters for PGNAA Applications

Ki-Yoon Lee[1], Kyung-Hwan Jung[1], Hyun-Dong Kim[1], Jun-Young Shin[2], Jung-Hyeon Eo[2], Jong-Yul Kim[3], Jin-Hyung Park[4]*, and Cheol-Ha Baek[1,5]*

[1]*Department of Health Medical Science, Kangwon National University, Samcheok 25949, Republic of Korea*
[2]*3I Solution Inc., Saneop-ro 156beon-gil, Suwon 16648, Republic of Korea*
[3]*Neutron Instrumentation Division, Korea Atomic Energy Research Institute, Daejeon 34057, Republic of Korea*
[4]*Advanced Radiation Technology Institute, Korea Atomic Energy Research Institute, Jeongeup 56212, Republic of Korea*
[5]*Department of Radiological Science, Kangwon National University, Samcheok 25949, Republic of Korea*

(Received 7 November 2025, Received in final form 22 December 2025, Accepted 22 December 2025)

Prompt Gamma Neutron Activation Analysis (PGNAA) is a non-destructive method for elemental analysis of bulk and heterogeneous materials and is widely used in industrial applications such as metal sorting and quality control. This work determines practical design parameters of a $LaBr_3$(Ce) scintillation detector—its thickness and angular placement—by explicitly addressing the trade-off between full-energy peak (FEP) efficiency and energy resolution. A hybrid Monte Carlo framework was developed, in which MCNP6 generates prompt gamma-ray source terms from neutron–sample reactions and GEANT4 simulates detector response including optical photon transport. The GEANT4 detector model was validated using a measured ^{137}Cs spectrum, and a Gaussian energy broadening (GEB) model calibrated for a 2″ × 2″ detector was incorporated to produce realistic spectra. For thicknesses of 1–4 inches and angles of 45°–180°, increasing thickness improved absolute efficiency but reduced light collection efficiency, resulting in degraded energy resolution; the 4-inch detector showed ~58% degradation in energy resolution than the 1-inch detector. In addition, the 180° configuration was excluded due to the elevated risk of neutron-induced activation when aligned with the beam axis. Considering both performance and engineering constraints, a 2-inch-thick detector positioned at 90° was selected as the best feasible configuration, providing a balanced efficiency–resolution performance and sufficient clearance for shielding and system integration. The proposed methodology offers practical guidelines for designing advanced PGNAA systems with geometry-dependent spectral performance.

Keywords : PGNAA, scintillator, Monte Carlo simulation, optimization, scrap metal recycling

1. Introduction

Prompt gamma-ray neutron activation analysis (PGNAA) is a non-destructive technique that determines elemental composition by measuring prompt gamma rays emitted immediately after thermal neutron capture (n, γ) and fast-neutron inelastic scattering (n, n′γ). PGNAA is particularly effective for large-volume bulk and heterogeneous samples, and it is therefore widely applied to industrial tasks such as metal scrap sorting, raw-material quality control, and process monitoring [1–5].

The analytical performance of PGNAA depends primarily on (i) detection efficiency for prompt gamma rays emitted from the sample, (ii) energy resolution of the detector, and (iii) suppression of neutron- and gamma-induced background. Among these factors, detector thickness and angular placement are key design parameters because they simultaneously affect full-energy peak (FEP) efficiency, spectral peak separation capability, and background tolerance.

$LaBr_3$(Ce) scintillators are well suited for PGNAA due to their high light yield (on the order of 6.3×10^4 photons/MeV), excellent intrinsic energy resolution (≈3% at 662 keV), and fast scintillation decay time (~20 ns) [6–8]. PGNAA covers an energy range from the keV scale up to several MeV; therefore, a minimum detector thickness is required to achieve sufficient FEP efficiency. However, as scintillator thickness increases, the mean optical path to the photosensor becomes longer and internal reflections increase, which can reduce the light collection efficiency

*Corresponding author: Tel: +82-63-570-3444
e-mail: jhpak@kaeri.re.kr
Tel: +82-33-540-3384, e-mail: baekch@kangwon.ac.kr

(LCE) [9, 10]. Reduced LCE decreases the number of collected photoelectrons and therefore worsens the statistical component of energy resolution.

Energy resolution in scintillation detectors is governed by multiple effects including material non-proportionality, electronic noise, and non-uniformity in light collection [11–13]. In practical detector optimization, thickness increases typically improve efficiency but can degrade LCE and thus energy resolution. Optimizing the trade-off between efficiency and resolution is therefore essential for improving PGNAA performance.

Conventional MCNP-based PGNAA studies accurately model neutron transport and nuclear reactions, but MCNP does not simulate optical-photon transport and thus cannot predict geometry-dependent light collection in scintillators beyond response-function approximations. As a result, many studies apply fixed Gaussian energy broadening (GEB) parameters (e.g., via FT8) calibrated for a single detector configuration [14]. However, this approach does not explicitly account for the physical coupling between geometric changes (e.g., thickness) and optical performance (LCE), which can systematically alter energy resolution during geometry optimization.

GEANT4 provides a validated optical-physics toolkit that can model scintillation photon generation and transport, including reflections, refraction, absorption, and surface/interface effects. This capability allows geometry-dependent LCE to be explicitly linked to energy-resolution predictions.

Accordingly, this study aims to identify practical design parameters—thickness and angular placement—of a cylindrical $LaBr_3$(Ce) scintillator for PGNAA by using a coupled MCNP6–GEANT4 framework that incorporates geometry-dependent optical effects into realistic spectral predictions.

2. Materials and Methods

2.1. Hybrid simulation framework

A hybrid simulation framework was developed by integrating GEANT4 (ver. 11.3.2) for optical photon transport and detector response with MCNP6 (ver. 6.3) for neutron transport and nuclear reaction source-term generation. MCNP6 was used to compute prompt gamma-ray emissions from neutron–sample interactions, while GEANT4 was used to (i) validate the reference $LaBr_3$(Ce) detector model against experimental data and (ii) simulate detector response under varying thickness and angle configurations.

MCNP6 employed neutron physics based on the ENDF/B-VIII.0 library and thermal scattering data S(α, β). GEANT4 used an electromagnetic physics list (G4EmStandardPhysics_option4) and optical physics (G4OpticalPhysics) to model optical photon generation and transport [15].

2.2. Monte Carlo model verification

The GEANT4 $LaBr_3$(Ce) detector model (Fig. 1) consisted of a 2-inch-diameter, 2-inch-long cylindrical $LaBr_3$(Ce) crystal, a PTFE (Teflon) diffuse reflector, a quartz window, a photocathode, and an aluminum housing.

To validate the detector response model, a ^{137}Cs source (662 keV) was simulated and compared with a measured spectrum obtained using a 2″ × 2″ $LaBr_3$(Ce) detector. From the measured spectrum, baseline GEB parameters (a_0, b_0, c_0) were derived for the energy–resolution relation:

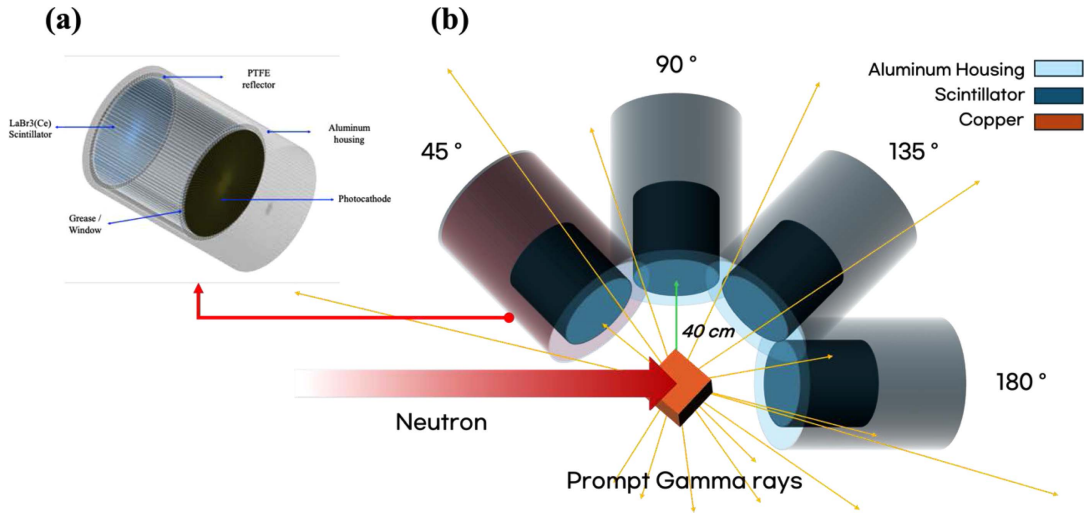

Fig. 1. (Color online) Schematic diagram of the $LaBr_3$(Ce) scintillation detector geometry modeled in GEANT4: (a) detector structure and (b) overall simulation layout and test cases.

$$FWHM(E) = \sqrt{a_0^2 + b_0 \cdot \mathrm{E} + \mathrm{c}_0 \cdot \mathrm{E}^2}\ (E\ in\ MeV) \quad (1)$$

In Eq. (1), a_0 represents configuration-dependent contributions dominated by electronic noise and light-collection non-uniformity, b_0 represents statistical fluctuations associated with photoelectron counting, and c_0 represents non-proportionality of the scintillator material [11–13]. These parameters were applied to GEANT4 energy-deposition results using a Gaussian smearing function. Agreement between simulated and measured spectra (peak width and spectral shape near the photopeak and Compton continuum) was used to confirm model reliability.

2.3. MCNP6-based PGNAA source-term generation

MCNP6 simulations modeled 0.025 eV thermal neutrons incident along the unit vector (1, 0, 0) from position (0, 5, 5) onto a copper sample represented as a 10-cm cube centered at (45, 5, 5) (Fig. 2).

To record prompt gamma rays from dominant reactions (n, γ) and (n, $n'\gamma$), we tracked neutrons and photons and enabled PTRAC to capture secondary-particle generation. From the PTRAC output, we extracted gamma-ray energy and direction vectors (E, x, y, z, u, v, w) with a Python script for use as an input source in GEANT4 detector-response simulations.

2.4. GEANT4 detector-response simulation using the MCNP PGNAA data

To simulate the detector response in the PGNAA environment, the prompt gamma-ray source term generated by MCNP6 was utilized as the input for the GEANT4 simulation. The geometry of the $LaBr_3$(Ce) scintillator was varied across four thicknesses (1, 2, 3, and 4 inches) and four angular positions relative to the neutron beam (45°, 90°, 135°, and 180°). For each angle, the center coordinates of the scintillator were adjusted to maintain a consistent distance from the Cu sample.

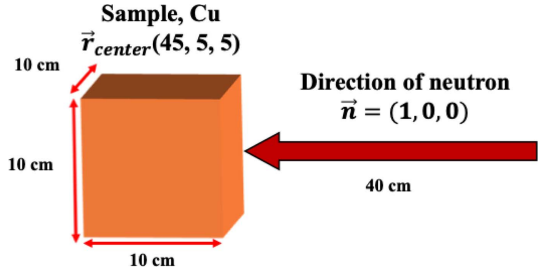

Fig. 2. (Color online) Configuration of the PGNAA simulation environment in MCNP6, illustrating the neutron beam trajectory and the copper sample position.

Consequently, the energy spectra and integrated photon counts were analyzed across a total of 16 geometric configurations (Fig. 1).

2.4.1. Performance metrics

For quantitative optimization, five key performance metrics were defined. The LCE represents the overall efficiency of converting scintillation photons into photoelectrons. It is defined as the ratio of the number of photoelectrons (N_{pe}) to the total number of generated scintillation photons (N_{scint}):

$$LCE = \frac{\mathrm{N_{pe}}}{N_{scint}} \quad (2)$$

The energy resolution is primarily governed by statistical fluctuations in the number of photoelectrons. The Statistical Resolution (R_{stat}) is defined as:

$$R_{stat} \approx \frac{2.355}{\sqrt{N_{pe}}} \quad (3)$$

The Geometric Resolution (R_{geom}) accounts for the resolution degradation caused by the geometric non-uniformity of light collection:

$$R_{geom} = \frac{2.355 \times \sigma_{geom}}{E_{dep}} \quad (4)$$

where σ_{geom} is the standard deviation of the energy deposition due to geometric effects, and E_{dep} is the mean deposited energy.

The detection efficiencies, Absolute Efficiency (Abs_{Eff}) and Peak Efficiency ($Peak_{Eff}$), are calculated as follows:

$$Abs_{Eff} = \frac{N_{total}}{N_{emit}}, \qquad Peak_{Eff} = \frac{N_{peak}}{N_{emit}} \quad (5)$$

where N_{total} is the total number of recorded pulses, N_{peak} is the count in the full-energy peak, and N_{emit} is the total number of gamma-rays emitted from the source.

2.4.2. Geometry-dependent GEB scaling strategy

To generate realistic energy spectra comparable to experimental conditions, a GEB function was applied to the ideal simulation outputs. The GEB parameters (a, b, c) for the 2-inch thickness were derived experimentally using standard gamma-ray sources, serving as the reference baseline. For the 1-, 3-, and 4-inch thicknesses, where direct experimental data were unavailable, the GEB parameters were estimated by scaling the baseline values according to the variations in the simulated optical characteristics, specifically the LCE and R_{stat}. Finally, these estimated parameters were convolved with the GEANT4 energy deposition data to produce the final

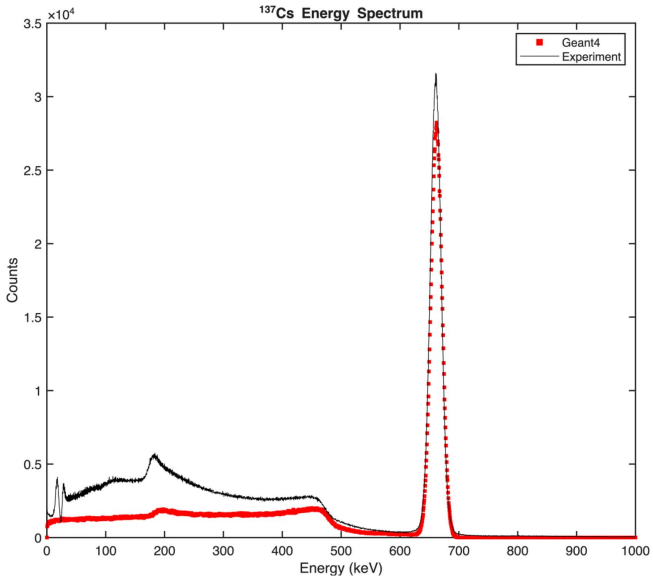

Fig. 3. (Color online) Comparison of the simulated energy spectrum (GEANT4) and experimental data for a ^{137}Cs source (662 keV) using a 2-inch detector.

energy spectra used for the comparative analysis.

3. Results and Discussion

3.1. GEANT4 model validation

Fig. 3 compares the GEANT4 simulation results, with the calibrated GEB parameters applied, against the experimentally detected energy spectrum of ^{137}Cs (662 keV) to verify the reliability of the GEANT4 simulation. At 662 keV, the Full Width at Half Maximum (FWHM) values were obtained as 22.06 keV for the GEANT4 simulation and 21.03 keV for the experimental data. The corresponding energy resolutions were 3.33% and 3.18%, respectively. This close agreement validates the reliability of the scintillator model implemented in the GEANT4 simulation.

3.2. MCNP6 PGNAA Radiation Field Data

Analysis of PTRAC data from MCNP6, which transported 100 million neutrons and recorded all reactions with the Cu sample, showed that 148,949,643 photons were recorded in the /ptrac/Bank events. From these events, gamma-ray energy and vector data (E, x, y, z, u, v, w) were extracted as sources in GEANT4.

Additionally, the reliability of MCNP6 was evaluated by comparing the energy spectrum of gamma rays emitted from neutron-sample nuclear reactions with PGNAA data for the element. The energy spectrum of gamma rays emitted from neutron-sample reactions, calculated using the F4 tally, is illustrated in Fig. 4. This spectrum does not reflect the physical and optical properties of the scintillator, such as the resolution of the $LaBr_3(Ce)$ scintillator, and thus differs from the actual spectrum detected by the $LaBr_3(Ce)$ scintillator.

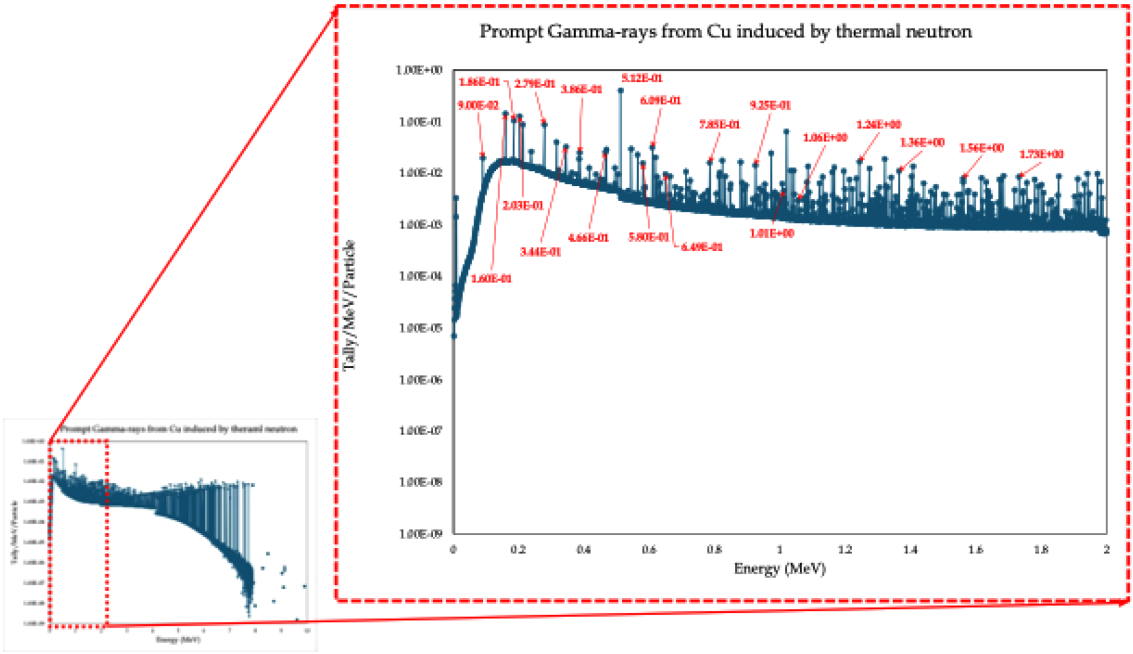

Fig. 4. (Color online) Prompt gamma-ray energy spectrum emitted from the copper (Cu) sample calculated using the PTRAC card in MCNP6.

Table 1. Comparison of prompt gamma-ray energy peaks and reaction cross-sections from reference and simulation by neutron reactions with Cu sample.

E_γ (keV)		σ_γ (b)	E_γ (keV)		σ_γ (b)
Reference	Simulation		Reference	Simulation	
89.08	90	0.097	608.766	609	0.270
159.281	160	0.648	648.80	649	0.102
185.96	186	0.244	770.6	785	17
202.950	203	0.193	924.5	925	1.5
278.250	279	0.893	1,013.5	1,012	1.6
343.898	344	0.215	1,050.7	1,068	2.6
385.77	386	0.131	1,357.9	1,360	0.40
465.14	466	0.135	1,558.2	1,560	0.80
579.75	580	0.089	1,724.9	1,730	4.0

Table 1 presents a comparison of the major prompt gamma-ray data for Cu calculated by MCNP6 against reference values from the Handbook of Prompt Gamma Activation Analysis with Neutron Beams [16] and the Atlas of Gamma-ray Spectra from the Inelastic Scattering of Reactor Fast Neutrons [17]. The simulation results demonstrate excellent consistency with these established datasets, confirming the reliability of the MCNP6 calculations. Key gamma-ray energies corresponding to high reaction cross-sections are summarized in the table.

3.3. Analysis of Simulation Results and Selection of Practical Optimization Conditions

GEANT4 simulations were performed for 16 geometric configurations to evaluate detector performance. Table 2 presents the normalized total scores derived from LCE, R_{stat}, R_{geom}, Abs_{Eff}, and $Peak_{Eff}$. The data clearly demonstrate a distinct trade-off among these performance metrics depending on the geometry.

Based on the normalized scoring analysis, configurations exhibiting unbalanced characteristics or operational risks were excluded from the optimization candidates.

First, the 1-inch thickness models achieved the highest scores (0.9–1.0) in optical metrics such as R_{stat} and R_{geom}. However, their Abs_{Eff} scores were notably low (approx. 0.3) compared to other thicknesses. This indicates an inability to secure sufficient valid signals, full-energy peak counts, required for PGNAA, leading to their exclusion despite superior resolution capabilities.

Conversely, the 3-inch and 4-inch thickness models obtained near-perfect efficiency scores (0.8–1.0) but suffered a sharp decline in LCE and R_{stat} (dropping to the 0.3–0.6 range). Although their Total Scores appeared high due to the dominant weighting of efficiency, this reflects a simplistic compensation where massive efficiency masks severe degradation in resolution. In PGNAA systems requiring precise nuclide identification, such degradation in energy resolution is unacceptable. Therefore,

Table 2. Comparison of Simulated Performance Metrics for LaBr3(Ce) Scintillator According to Thickness and Angle in PGNAA (Normalized).

Thickness (inch)	Angle (deg)	LCE (%)	R_{stat} (%)	R_{geom} (%)	Abs_{Eff} (%)	$Peak_{Eff}$ (%)	Total Score
1	45	0.9109	0.9588	0.8779	0.3947	0.2967	3.4390
	90	0.9163	0.9299	0.8482	0.3608	0.2856	3.3408
	135	0.9096	0.9536	0.8712	0.3123	0.2825	3.3292
	180	1.0000	1.0000	0.9214	0.3093	0.2835	3.5142
2	45	0.6274	0.7700	0.9125	0.5986	0.5457	3.4542
	90	0.6167	0.7655	0.9027	0.4708	0.4776	3.2333
	135	0.6287	0.7640	0.9067	0.4775	0.4370	3.2139
	180	0.7995	0.8657	0.9956	0.4114	0.4228	3.4950
3	45	0.4723	0.6594	0.8928	0.7959	0.8130	3.6334
	90	0.4371	0.6458	0.9050	0.5443	0.5549	3.0871
	135	0.4743	0.6576	0.8830	0.6406	0.5518	3.2073
	180	0.7092	0.8027	1.0000	0.4752	0.5203	3.5074
4	45	0.3701	0.5845	0.8355	1.0000	1.0000	3.7901
	90	0.3134	0.5518	0.8650	0.6008	0.5681	2.8991
	135	0.3723	0.5822	0.8298	0.8054	0.7449	3.3346
	180	0.6693	0.7668	0.9963	0.5248	0.5315	3.4887

Table 3. Estimated Gaussian Energy Broadening (GEB) Parameters (a, b, c) Based on Simulated Optical Characteristics for Each Thickness.

Thickness (inch)	GEB Parameters			Remark
	a	b	c	
1	0.001528	0.000510	0.00000975	Estimated (R_{stat} Ratio: 0.803)
2	0.001528	0.000790	0.00000975	Experimental Baseline
3	0.001528	0.001077	0.00000975	Estimated (R_{stat} Ratio: 1.168)
4	0.001528	0.001371	0.00000975	Estimated (R_{stat} Ratio: 1.317)

models with optical performance below a critical threshold were excluded, regardless of their efficiency scores.

Additionally, the 180° configuration was discarded despite its high efficiency scores. This geometry aligns the detector directly with the neutron beam axis, leading to a high risk of neutron-induced activation in the scintillator, which would increase background noise and deteriorate signal quality [18]. Considering the operational stability required for PGNAA, this configuration was deemed unsuitable.

Consequently, the 2-inch thickness model demonstrated the most balanced distribution between efficiency scores (0.4–0.6) and resolution scores (0.7–0.8). Regarding angular placement, while the 45° angle is theoretically superior, the 2-inch at 90° configuration was selected as the pragmatic alternative to accommodate physical constraints in the experimental setup. It provides a balanced performance profile, maintaining better LCE compared to the 3-inch model at the same angle while offering superior accessibility.

To generate realistic energy spectra, the GEB parameters (a, b, c) were calculated for each thickness. Using the experimental values of the 2-inch thickness as a baseline, the parameters for other thicknesses were estimated by scaling the statistical term based on the squared ratio of simulated R_{stat} values (Table 3).

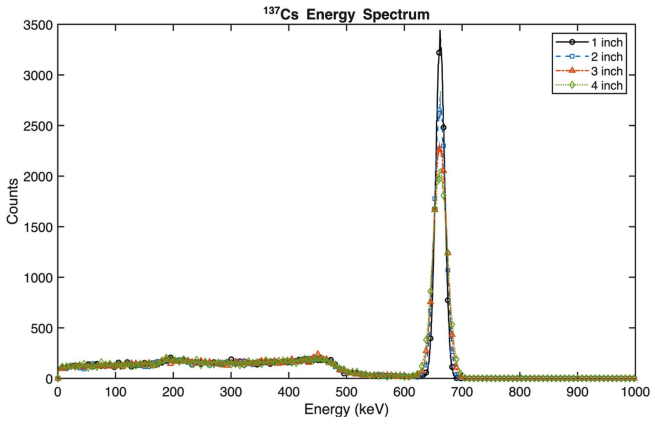

Fig. 5. (Color online) Energy spectra of ^{137}Cs generated by applying the GEB parameters (a, b, c) estimated for each scintillator thickness based on the performance metrics.

3.4. Generation of GEB-Convolved Energy Spectra and Performance Verification

The GEB parameters (a, b, c) calculated for each scintillator thickness in Section 3.3 were applied to the GEANT4 simulation to evaluate the variations in energy resolution and FWHM with increasing thickness. The resulting energy spectra for ^{137}Cs (662 keV) according to scintillator thickness are presented in Fig. 5, and the corresponding energy resolution and FWHM values are summarized in Table 4. The analysis confirmed a distinct degradation in energy resolution as the scintillator thickness increased. Specifically, the energy resolutions of the 3-inch and 4-inch scintillators were 4.08% and 4.47%, respectively. This represents a performance degradation of approximately 45% and 58%, respectively, compared to the 1-inch model (2.82%). This finding suggests that the reduction in light collection efficiency associated with increased thickness is a primary factor driving the deterioration of resolution.

Based on the normalized scoring analysis in Section 3.3, the optimal angular conditions for each thickness were identified as 45° for the 1-, 3-, and 4-inch models, and 90° for the 2-inch model. To evaluate the spectral discrimination capability across thicknesses, the prompt gamma-ray energy spectra of Copper (Cu) were compared at a fixed angle of 45°, as illustrated in Fig. 6. The comparison revealed that the 1-inch and 2-inch models,

Table 4. Comparison of FWHM and Energy Resolution at 662 keV (137Cs) According to Scintillator Thickness Using Derived GEB Parameters (a, b, c).

Thickness (inch)	Peak (keV)	FWHM (keV)	Energy Resolution (%)
1	662.5	18.668	2.81
2	662.5	22.060	3.33
3	661.25	26.986	4.08
4	662.75	29.592	4.46

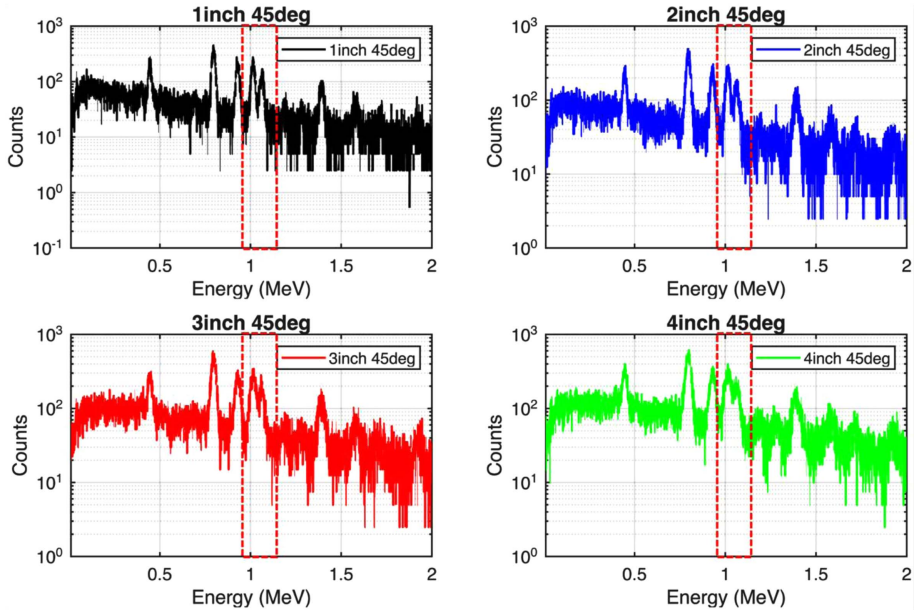

Fig. 6. (Color online) Comparison of GEB-convolved prompt gamma-ray energy spectra of Copper (Cu) at a fixed angle of 45° for different $LaBr_3$(Ce) thicknesses: (a) 1-inch, (b) 2-inch, (c) 3-inch, and (d) 4-inch.

with their superior energy resolution, could clearly distinguish two adjacent peaks near 1 MeV. In contrast, the 3-inch and 4-inch models—particularly the 4-inch case—failed to resolve these peaks due to excessive energy broadening caused by poor resolution. Consequently, the 3-inch and 4-inch thicknesses were excluded from the optimal candidates. Furthermore, the 1-inch thickness was also excluded despite its excellent resolution, as its thin profile resulted in low absolute detection efficiency and full-energy peak efficiency, making it difficult to secure sufficient valid signals. As a result, the 2-inch thickness was determined to be the optimal thickness, offering the best balance between resolution and efficiency.

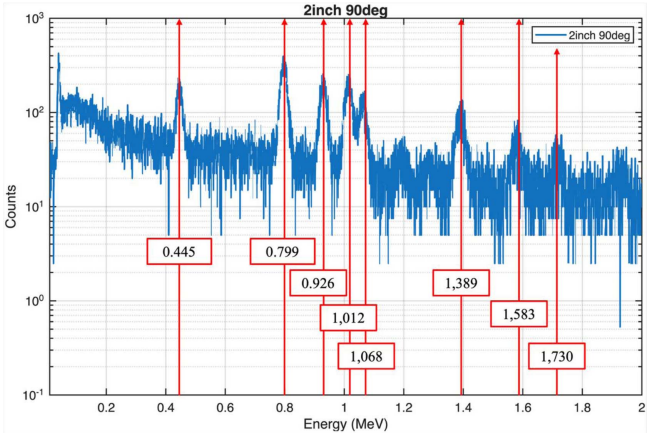

Fig. 7. (Color online) GEB-convolved prompt gamma-ray energy spectrum of Copper (Cu) obtained from the optimized geometric configuration (2-inch thickness at 90°).

Regarding the angular placement for the selected 2-inch thickness, the 180° configuration was excluded because the direct alignment of the scintillator with the neutron beam significantly increases the probability of neutron-induced activation within the crystal. This phenomenon can lead to increased background noise and a deterioration in signal quality. Therefore, as indicated in Table 2, the 90° configuration was selected as the optimal angle for the 2-inch thickness. The Cu prompt gamma-ray energy spectrum obtained under this final condition (2-inch at 90°) is shown in Fig. 7. In this spectrum, the peaks estimated to be characteristic Cu prompt gamma-ray energy peaks were clearly identified at 445, 799, 926, 1,012, 1,068, 1,389, 1,583, and 1,730 keV.

4. Conclusions

In this study, the geometric configuration of a $LaBr_3$(Ce) scintillator for a PGNAA system was optimized using a coupled MCNP6 and GEANT4 simulation framework. To ensure realistic performance prediction, a GEB correction model was applied, utilizing parameters estimated from experimental data and scaled by simulated optical characteristics.

The results identified a distinct trade-off between detection efficiency and optical performance. While increasing the scintillator thickness improved absolute efficiency, it concurrently reduced the LCE, leading to a

severe degradation in energy resolution. Specifically, the 4-inch model, despite having the highest efficiency, suffered from excessive peak broadening that hindered the separation of adjacent copper (Cu) peaks, showing a resolution degradation of approximately 58% compared to the 1-inch model. Furthermore, the 180º configuration was excluded due to the high risk of neutron-induced activation caused by direct alignment with the neutron beam.

Although the 3-inch thickness at 45º was the theoretical optimum, the 2-inch thickness at 90º was selected as the optimal practical configuration to accommodate spatial constraints and ensure precise peak identification. Analysis confirmed that the selected 2-inch-90º configuration provides a balanced performance with sufficient sensitivity and excellent energy resolution to clearly identify characteristic peaks. Therefore, the optimal design parameters for the $LaBr_3$(Ce) scintillator proposed in this study are expected to be effectively utilized in future experiments for system construction and performance verification, satisfying both cost-effectiveness and analytical precision.

Acknowledgments

This research was supported by the Technology Development Program of the Ministry of SMEs and Startups [RS-2024-00469068].

References

[1] H. Folz, J. Henjes, A. Heuer, J. Lahl, P. Olfert, B. Seen, S. Stabenau, K. Krycki, M. Lange-Hegermann, and H. Shayan, arXiv preprint arXiv:2404.14107 (2024).
[2] J. Roult, C. Carasco, L. Loubet, B. Pérot, L. Tamagno, D. Etasse, M. Frank, A. Havenith, and J. Collot, 2022 IEEE Nuclear Science Symposium and Medical Imaging Conference (NSS/MIC), IEEE (2022).
[3] A. A. Naqvi, M. M. Nagadi, and O. S. B. Al-Amoudi, Nuclear Instruments and Methods in Physics Research Section B: Beam Interactions with Materials and Atoms **225**, 331 (2004).
[4] H. Kurth, In International Symposium on Nickel and Cobalt, Cham: Springer Nature, Switzerland (2025).
[5] H. Shayan, K. Krycki, M. Doemeland, and M. Lange-Hegermann, IEEE Transactions on Nuclear Science **70**, 6 (2023).
[6] R. Nicolini, F. Camera, N. Blasi, S. Brambilla, R. Bassini, C. Boiano, A. Bracco, F. C. L. Crespi, O. Wieland, G. Benzoni, S. Leoni, B. Million, D. Montanari, and A. Zalite, Nuclear Instruments and Methods in Physics Research Section A: Accelerators, Spectrometers, Detectors and Associated Equipment. **582**, 554 (2007).
[7] F. Quarati, A. J. J. Bos, S. Brandenburg, C. Dathy, P. Dorenb, S. Kraft, R. W. Ostendorf, V. Ouspenski, and A. Ownes, Nuclear Instruments and Methods in Physics Research Section A: Accelerators, Spectrometers, Detectors and Associated Equipment **574**, 115 (2007).
[8] A. Favalli, H. C. Mehner, V. Ciriello, and B. Pedersen, Applied Radiation and Isotopes **68**, 901 (2010).
[9] G. F. Knoll, T. F. Knoll, and T. M. Henderson, IEEE Transactions on Nuclear Science **35**, 872 (2002).
[10] W. C. Chuirazzi and E. C. Aaron, Journal of Imaging **6**, 56 (2020).
[11] W. W. Moses, S. A. Payne, W. S. Choong, G. Hull, and B. W. Reutter, IEEE Transactions on Nuclear Science **55**, 1049 (2008).
[12] M. Moszyński, Radiation Measurements **45**, 372 (2010).
[13] P. Dorenbos, J. Th. M. de Haas, and C. W. E. Van Eijk, IEEE Transactions on Nuclear Science **42**, 2190 (1995).
[14] T. Wilcox, ANS RPSD-2014, LA-UR-14-27128 (2014).
[15] https://GEANT4.web.cern.ch
[16] G. L. Molnár, Handbook of Prompt Gamma Activation Analysis: With Neutron Beams. Vol. 1. Springer Science & Business Media, Berlin (2004) pp. 252-253.
[17] A. M. Demidov, L. I. Govor, Yu. K. Cherepantsev, M. R. Ahmed, S. Al-Najjar, M. A. Al-Amili, N. Al-Assafi, and N. Rammo, Atlas of gamma-ray spectra from the inelastic scattering of reactor fast neutrons. Moscow: Atomizdat, Moscow (1978) pp. 77-81.
[18] Y. Lu, Z. H. Song, G. Li, X. J. Tan, X. C. Zhao, and K. Zhang, Chinese Physics C **39**, 10 (2015).